ACS chemical biology

Letters

pubs.acs.org/acschemicalbiology

X-ray Structures of Human Furin in Complex with Competitive Inhibitors

Sven O. Dahms,*[,†] Kornelia Hardes,[‡] Gero L. Becker,[‡] Torsten Steinmetzer,[‡] Hans Brandstetter,[§] and Manuel E. Than*[,†]

[†]Protein Crystallography Group, Leibniz Institute for Age Research-Fritz Lipmann Institute (FLI), Beutenbergstr. 11, 07745 Jena, Germany

[‡]Department of Pharmaceutical Chemistry, Philipps University Marburg, Marbacher Weg 6, D-35032 Marburg, Germany

[§]Department of Molecular Biology, University of Salzburg, Billrothstrasse 11, A-5020 Salzburg, Austria

Supporting Information

ABSTRACT: Furin inhibitors are promising therapeutics for the treatment of cancer and numerous infections caused by bacteria and viruses, including the highly lethal *Bacillus anthracis* or the pandemic influenza virus. Development and improvement of inhibitors for pharmacological use require a detailed knowledge of the protease's substrate and inhibitor binding properties. Here we present a novel preparation of human furin and the first crystal structures of this enzyme in complex with noncovalent inhibitors. We show the inhibitor exchange by soaking, allowing the investigation of additional inhibitors and substrate analogues. Thus, our work provides a basis for the rational design of furin inhibitors.

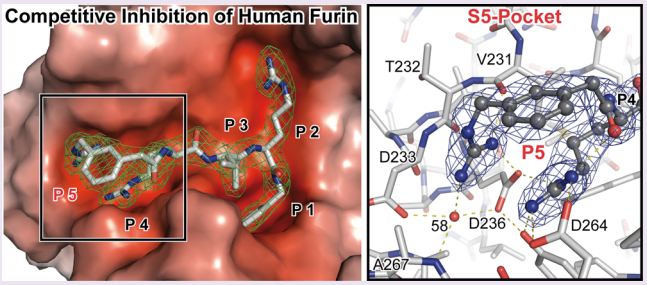

Furin is a member of the pro-hormone/pro-protein convertase family (PCs) of subtilisin-like endoproteinases.[1] PCs are required for activation and maturation of many secreted proteins. Target proteins include peptide hormones, growth factors, matrix metalloproteases, blood clotting factors, regulators of the cholesterol metabolism, bacterial toxins, and viral capsid proteins.[2,3] Therefore furin and other PCs are intensively investigated as pharmacological targets for the treatment of many diseases, e.g., atherosclerosis, hypercholesterolaemia, and cancer, as well as viral and bacterial infections.[4] Proteolysis by furin is highly specific and occurs C-terminal to a multibasic recognition motive. The extended substrate binding site gives rise to diverging specificities, strongly favoring arginine at P1 and basic amino acid side chains at P2, P4, and/or P6, whereby R-[X]-(R/K)-R↓ is the most common recognition sequence.

Up to now several compound classes have been identified as promising starting points for drug development. In addition to small molecules and peptide based inhibitors,[5] also camelid VHH-antibodies were found to selectively inhibit furin.[6] It was shown that furin inhibitors are indeed suitable to prevent the growth and invasiveness of tumors (e.g., refs 7 and 8), the replication of viruses (e.g., refs 9 and 10), or the toxicity of bacterial toxins (e.g., refs 11 and 12). For their broad pharmacological application, next generation compounds require, however, improvements of their stability, selectivity, bioavailability, and/or pharmacokinetics.[5]

Structure-guided drug design provides the possibility for rational modification and directed development of enhanced inhibitors. This approach requires an in-depth structural understanding of furin−inhibitor complexes. So far, structures of mouse furin[13] and of its yeast homologue kexin[14] are available only in complex with covalently attached peptides. The mouse furin structure showed the interaction with a prototypical R-V-K-R↓ recognition motive. Investigation of other furin substrate analogues or inhibitors by exchange of the initially co-crystallized compound, however, was not possible.

Peptidomimetic compounds based on a phenylacetyl-Arg-Val-Arg-4-(amidomethyl)benzamidine (Phac-RVR-4-Amba) core structure [15] belong to the strongest noncovalent inhibitors available so far. Upon variation of the P5 position, dramatic changes of the K_i values were observed that cannot be explained by the known recognition motive. The K_i improved by approximately 2 orders of magnitude after addition of basic substituents, e.g., by modification of the Phac-moiety at P5 by a *m*- or *p*-guanidinomethyl group.[15]

Here we describe a novel preparation of human furin and two crystal structures of this enzyme in complex with competitive, noncovalent inhibitors. The tight binding observed for the inhibitor complexes is accompanied by a very strong increase of the structural stability in thermal denaturation experiments. The structures explain the different affinities of the

Received: February 4, 2014
Accepted: March 25, 2014
Published: March 25, 2014

   dx.doi.org/10.1021/cb500087x | ACS Chem. Biol. 2014, 9, 1113−1118

inhibitors and the related specificity of the protease for substrates with Arg/Lys residues at the P5 position.

We have developed a novel preparation of human furin and solved the first structures of a PC in complex with noncovalent, competitive inhibitors, a prerequisite for the structure based development of next generation compounds. The interaction of the substrate mimetic inhibitor within the active site cleft of furin revealed so far exclusive insights about specificity determinants beyond the S4 pocket.

Purification and Crystallization. Successful crystallization of human furin required the development of a novel expression and purification procedure to obtain highly homogeneous protein samples. For this purpose, a minimal, C-terminally 6xHis-tagged construct (Asp23−Ala574) was designed for transient expression in human embryonic kidney cells (HEK293). A specialized HEK293S Gnt$^-$ cell line[16] was used to produce human furin with homogeneous termini and a uniform glycosylation. An efficient, ∼300-fold enrichment of the active protease from a fetal bovine serum (FBS) rich medium was achieved with a three-step affinity chromatography scheme, including immobilized metal affinity purification (IMAC) and inhibitor based affinity purification[17] (Supplementary Figure 1). Typically, 1−2 mg of purified enzyme was obtained per liter of conditioned cell culture medium. The described expression and purification procedure can readily be adapted to the large-scale preparation of other PCs in the future. The herein produced, homogenously glycosylated, recombinant human furin showed inhibition constants very similar to those of the complex glycosylated enzyme used in previous studies (Supplementary Table 1; refs 10 and 15).

Overall Structure. Furin was crystallized in the presence of *m*-guanidinomethyl-Phac-RVR-Amba (I1, Figure 1a, ref 15). The crystals belong to the orthorhombic spacegroup $P2_12_12_1$. The structure of the furin−I1 complex was solved by molecular replacement with mouse furin as search model (PDB-ID 1P8J, ref 13) and refined to 2.3 Å resolution (Figure 1b, Table 1). The asymmetric unit contains six copies of the protease−inhibitor complex arranged in three pairs. The active site of all protomers is solvent-exposed and allows the exchange of the inhibitor in soaking experiments (see below). All six human furin molecules are nearly identical (∼0.05 Å RMSD of their Cα positions in multiple structural alignments with PDBeFold[18]). Structural alignments of human and mouse furin revealed average RMSD values of 0.5 Å, showing a high overall similarity for the catalytic domain and P-domain between the homologues. Sites of single amino acid substitutions between the homologues were well-defined in the difference electron density map (Supplementary Figure 2) and do not affect the overall fold. The human structure supports the previously modeled specificity determinants at P1′ and P2′[19] and allows to further study, e.g., the structural impact of single nucleotide polymorphisms in furin and other PCs, reported to play a role in diabetes and obesity.[20]

In addition to the previously described calcium-binding sites 1 and 2 (Ca1, Ca2[21]), further metal-binding sites were identified in the structure of human furin (Figure 1b, Supplementary Figure 3a−c) and validated using CheckMyMetal.[22] The newly identified calcium binding site 3 (Ca3) is located at the surface of the protein (Supplementary Figure 3c). It is coordinated by the side chains of Asp174, Asp179 (bidendate), the carbonyl oxygen of Asp181, as well as three solvent molecules and adopts a typical pentagonal bipyramidal arrangement (average bond distance 2.5 Å). Near to the active site cleft we identified a Na^+-binding site, indicated by a spherical electron density surrounded by five oxygen atoms, Thr314 OH, Thr314 O, Ser311 O, Thr309 O, and an internal solvent molecule (Supplementary Figure 4; average metal−oxygen distance 2.38 Å). Na1 was also observed in the structure of the yeast homologue kexin.[23] The relative position of Na1 with respect to the active site mirrors that found in thrombin and related coagulation proteases.[24] This finding points toward another intriguing example of convergent evolution of trypsin- and subtilisin-like serine proteases.[25] Interestingly, the metal binding sites Ca1, Ca3, and Na1 of human furin are also found in the catalytic domain of the thermostable subtilisin-like protease thermitase.[26]

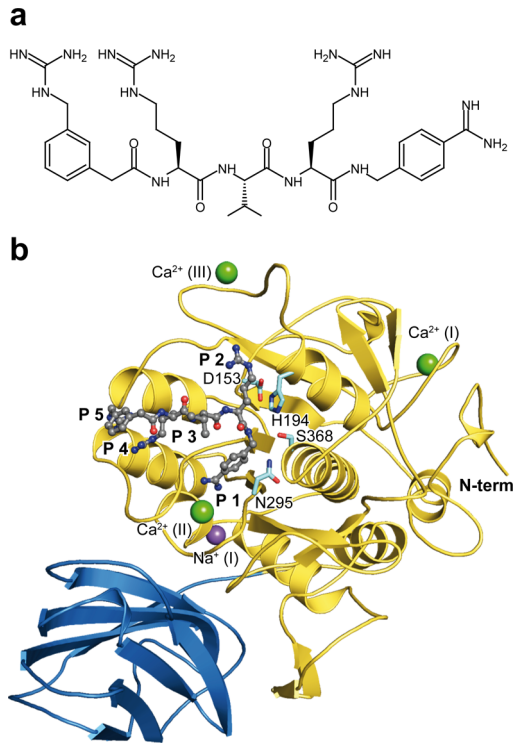

Figure 1. Structure of human furin in complex with inhibitor I1. (a) *m*-Guanidinomethyl-phenylacetyl-Arg-Val-Arg-(amidomethyl)-benzamidine (*m*-guanidinomethyl-Phac-RVR-Amba, I1). (b) Human furin is shown as a cartoon representation. The catalytic domain and the P-domain are colored in yellow and blue, respectively. The side chains of the catalytic triade (Ser368, His194, and Asp153) and of the oxyanion hole (Asn295) are shown as sticks (cyan carbon atoms). The inhibitor (ball and stick representation, gray carbon atoms) interaction sites are numbered P1−P5. Bound calcium and sodium ions are given as green and purple spheres, respectively.

Competitive Inhibition of Human Furin. Different from the covalently inactivated PC structures available so far, the catalytic triade of human furin adopts a conformation that shows the residues Ser368 and His194 in tight hydrogen-bonding distance as expected for a respective proton transfer and the nucleophilic attack at the substrate's scissile peptide bond (Figure 2a). The oxy-anion hole is occupied by the well-defined water molecule 701, bridging Ser368 and Asn295. Inhibitor I1 contains a C-terminal Amba headgroup at the P1 position, mimicking the preferred arginine side chain found here for most of the natural furin substrates. Similar to arginine, Amba deeply inserts into the S1 pocket (Supplementary Figure 5), forming tight hydrogen bonds with the carbonyl oxygen atoms of Pro256 and Ala292 as well as electrostatic interactions

dx.doi.org/10.1021/cb500087x | *ACS Chem. Biol.* 2014, 9, 1113−1118

Table 1. Data Collection Statistics

	I1	I2
data collection		
wavelength (Å)	0.918	
space group	$P2_12_12_1$	
unit cell parameters a (Å), b (Å), c (Å)	141.18, 152.85, 168.31	141.62, 152.61, 168.54
resolution range[a] (Å)	50.0−2.3 (2.44−2.30)	50.0−2.7 (2.86−2.7)
R_{pim}[a,b] (%)	7.2 (30.5)	7.9 (28.0)
R_{meas}[a] (%)	13.9 (59.7)	15.2 (52.6)
$I/\sigma I$[a]	9.7 (2.6)	9.7 (2.8)
completeness[a] (%)	99.4 (98.5)	99.5 (99.0)
obs: total/unique	610,835/160,915	377,299/100,092
refinement		
R_{work}/R_{free}	18.5/21.6	19.3/21.8
nonhydrogen atoms	23,098	22,347
protein/inhibitor/other	21,332/324/1442	21,332/294/721
B-factors (Å^2)		
overall/Wilson plot	26.7/31.4	23.6/26.8
protein/inhibitor/other	26.6/22.3/29.9	23.7/22.1/22.2
RMSD bond length (Å)	0.0079	0.0068
RMSD bonded B-factors (Å^2)	2.5	2.0

[a]Highest resolution shell is given in parentheses. [b]Calculated in SCALA in the resolution ranges (given in Å) 50−2.31 (2.43−2.31) and 50−2.71 (2.86−2.71) for I1 and I2, respectively.

with Asp306 (Figure 2a). The Amba group mediates extensive van der Waals interactions, resulting in tight enclosure of the planar phenyl ring by the peptide bonds Ser253−Gly255 on one side and the peptide bonds encompassing Gly294 on the other side (Figure 2a). In addition, the loss of entropy upon fixation to the S1 pocket is expected to be lower for Amba compared to more flexible moieties such as arginine. The tight interactions observed in the structure are in excellent agreement to kinetic studies, showing an increase of the inhibition potency of approximately 2 orders of magnitude, if the decarboxylated arginine derivative agmatine is replaced by Amba at P1.[10]

Binding of the P2 arginine side chain at the S2 pocket of furin requires electrostatic interactions, mediated by the conserved Asp154 (Figure 2b). In addition direct and water-bridged hydrogen bonds are formed to Asn192 and Asp228, respectively. The latter contact is replaced by a hydrogen bond to the carbonyl oxygen of Asp191, if lysine binds to the S2 pocket in mouse furin.[13] Similar observations were reported for the P2 interactions of kexin,[23] explaining the tolerance for arginine or lysine at P2 by furin and kexin.

P3 and P4 of inhibitor I1 adopt a conformation nearly identical to that of the covalently attached dec-RVKR-chloromethylketone peptide in mouse furin (Figure 2b,c, Supplementary Figure 5). The backbone interactions between I1 and Trp254-Pro256 of the protease place the inhibitor in a position to cover a hydrophobic patch at the bottom of the substrate binding cleft. The unusual conformation of the arginine side chain at P4 is primarily stabilized by charged hydrogen bonds to Glu236, Asp264, and Tyr308. In kexin completely different contacts were observed at the S4 pocket, showing major differences in the conformation of the protein backbone between Asp249−Ala256.[23]

S5 Site. The N-terminal guanidinomethyl group of I1 stacks parallel to the peptide bond Thr232−Asp233 (Figure 2c). This region of furin was originally predicted to act as an S6 pocket in a canonical substrate−protease interaction mode.[19] Electrostatic interactions are formed to Asp236, which is shared by this unusual S5 and the S4 pockets. Additionally, hydrogen bonds are formed to the backbone carbonyl of Val231 and a bound water molecule 715. This water molecule is also found in the unoccupied S5 pocket of the mouse furin-dec-RVKR-chloromethylketone complex (PDB-ID 1P8J, ref 13), interacting with Asp233, Asp236, and the amide of Ala267. This binding mode of the P5 side chain was completely unexpected and was not predicted by any modeling approach so far. In fact, the positively charged P4 and P5 guanidino groups are only approximately 4 Å apart. The strongly negative potential of furin's substrate binding pocket, however, facilitates charge equalization and thereby permits formation of a strong hydrogen-bonding network. In this way the P4−P5 combination interacts with the shared S4−S5 site of the protease in a key-lock mechanism, without necessity for any conformational rearrangements. Such a binding mode seems possible for any positively charged moiety at P5 that can adapt an extended conformation to interact with Asp236 and Val231 O. Indeed, kinetic studies demonstrated that the length and the conformational flexibility of the P5 substituent strikingly influence the K_i value.[15] Correspondingly, a change of the guanidinomethyl group from the meta to the para position results in similar binding properties with a change of the K_i from 16.7 ± 0.6 pM to 9.7 ± 1.5 pM (Supplementary Table 1). A largely decreased binding strength (K_i = 196 ± 15.2 pM) is observed, however, if a less extended *o*-guanidinomethyl-Phac moiety is placed at P5.

Inspection of the furin substrate database FurinDB[27] for the occurrence of basic amino acid side chains at P5 revealed a frequency of 0.33, which compares to a frequency of only 0.25 for their occurrence at P6. Interestingly, 93% of the substrates that have arginine or lysine residues at P5 also contain an arginine side chain at P4. Such recognition sequences are found for substrates that are cleaved by furin with high efficiency, e.g., for hemagglutinin of the highly infectious avian influenza virus strain H5N1, or in both self-activation sites inside the furin pro-domain.[27]

Next we compared the effect of inhibitors on the overall structural stability of human furin by inspection of their melting

dx.doi.org/10.1021/cb500087x | ACS Chem. Biol. 2014, 9, 1113−1118

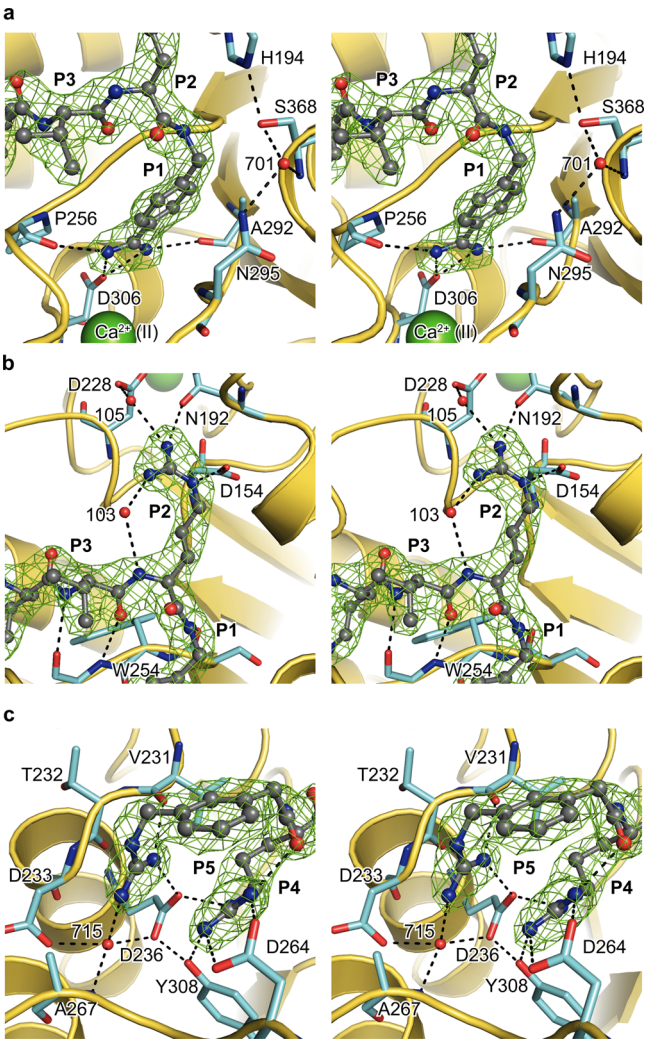

Figure 2. Detailed view of the furin–I1 interaction sites. The furin–inhibitor complex is shown in standard orientation as in Figure 1. In the stereo panels the Cα-carbon trace of the protease is given as cartoon representation (yellow). The inhibitor and important residues of furin are shown in dark gray (ball and stick model) and in cyan (stick model), respectively. Selected water molecules are shown as red spheres. Important interactions are highlighted with black dashes. The $F_o - F_c$ difference electron density omit map of the inhibitor (green mesh) is contoured at 3.5 σ. (a) The S1 pocket of the protease, interacting with the (amidomethyl)benzamidine-P1 moiety of I1. Ca^{2+} II at the bottom of the S1 pocket is shown as a green sphere. (b) The P2- and the P3-residues of the inhibitor. (c) Interactions of the P4-residue and of the P5-*m*-guanidinomethyl-phenylacetyl moiety of I1.

temperatures, T_m, in thermal denaturation assays (Figure 3). Whereas the uninhibited enzyme shows a T_m of 54.1 ± 0.1 °C, this value is increased to a T_m of 68.0 ± 0.3 °C in the presence of I1. Addition of Phac-RVR-Amba (I2, Figure 4a) that lacks the guanidinomethyl group at P5 resulted in an intermediate melting temperature of 62.5 ± 0.1 °C. These values correlate well with the corresponding K_i values, which were determined to be 16.7 ± 0.6 pM and 977 ± 196 pM for I1 and I2, respectively (Supplementary Table 1). Consequently, the interactions at the S5 pocket of the active site contribute largely to a global stabilization of the protease. Interestingly, it has been demonstrated that thermal stability is directly related to the crystallizability of proteins. We hence presume that the

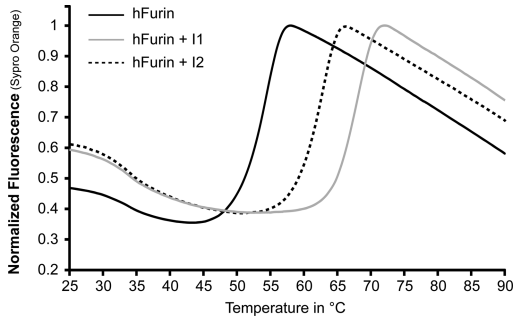

Figure 3. Gain of global structural stability upon inhibitor binding by human furin. Melting curves were determined based on the fluorescence of the dye Sypro Orange in dependence on the temperature.

stabilizing effect of I1 also largely improved the tendency of human furin to form well-ordered crystals.

Exchange of the Inhibitor by Soaking. During the past two decades a number of inhibitors have been developed, targeting furin and other PCs.[5] However, these compounds require improvements in specificity, affinity, pharmacokinetics, or bioavailability for therapeutic use, calling for a detailed understanding of the interactions of the PCs with substrates and inhibitors at their active site cleft. Especially specificity determinants beyond the canonical multibasic recognition sequence from P1 to P4 are poorly understood, although this is a highly promising target region for the development of inhibitors that selectively bind to specific PC family members.[19] Therefore a general applicable procedure for the structural investigation of furin–inhibitor or furin–substrate interactions is highly needed. The crystals of the noncovalent furin–I1 complex described in this study are very well suited for the exchange of I1 in soaking experiments with other inhibitors or substrate analogues, binding to the active site. To demonstrate the general applicability of this approach, we incubated the furin–I1 crystals with I2. Indeed, the electron density at the P5 position disappeared upon treatment of the crystals with excessive amounts of I2, indicating displacement of the initially co-crystallized inhibitor I1 (Figure 4b). Calculation of an isomorphous difference electron density between the data sets collected before and after soaking unambiguously confirmed the replacement of I1 by I2 (Figure 4b). In addition to the guanidinomethyl group no electron density was observed for the phenyl ring of the phenylacetate moiety of I2. The reason for the disappearance of its electron density is most likely a gain of flexibility in rotation upon the loss of the interactions to the S5 pocket. This lack of specific interactions of the unsubstituted aromatic Phac residue explains the decreased inhibitor potency of I2 and related compounds, containing aliphatic acyl groups (C2 to C10) at the N-terminus.[15]

The displacement of the highly potent inhibitor I1 by competitive soaking with excessive amounts of the less potent I2 is in excellent agreement with the binding mode found for the furin–I1 complex structure. I1 binds to the active site in a key-lock mechanism (see above), facilitating fast, diffusion-controlled binding kinetics. The occupation of the substrate-binding pocket of human furin is controlled only by the concentration and by the binding constant of the compound of interest. Hence the furin–I1 crystals are well suited for structural investigation of weak binding compounds by simple soaking in excessively concentrated solutions.

dx.doi.org/10.1021/cb500087x | *ACS Chem. Biol.* 2014, 9, 1113–1118

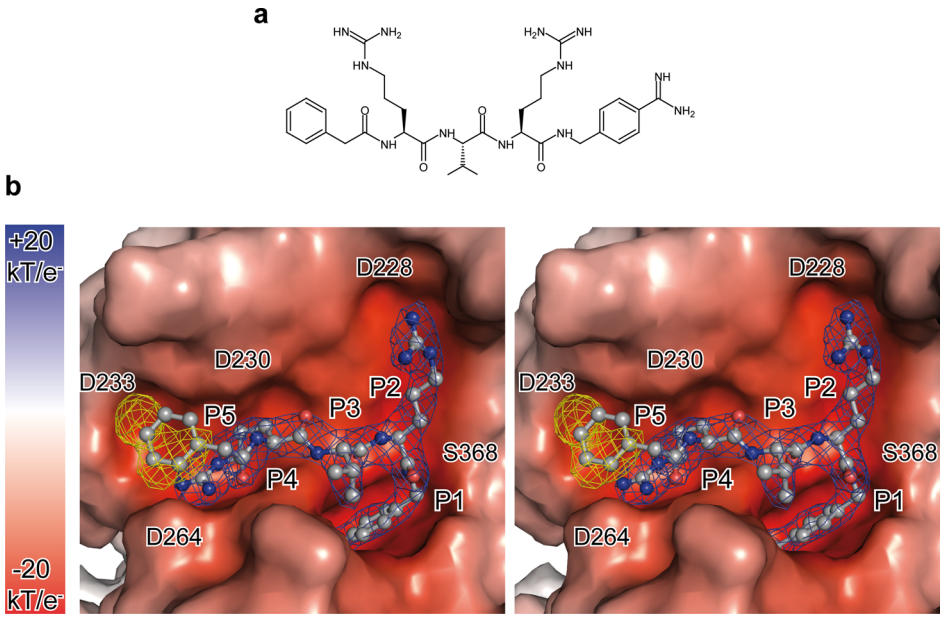

Figure 4. Exchange of the co-crystallized inhibitor I1 by soaking with I2. (a) Phenylacetyl-Arg-Val-Arg-(amidomethyl)benzamidine (Phac-RVR-Amba, I2). (b) Stereo representation of the sovent-accessible surface of the active site cleft of human furin, colored by the electrostatic potential. Inhibitor I2 is shown in standard orientation and is given as a ball and stick model in gray. The residues of the inhibitor are numbered (P1−P5). The $F_o - F_c$ difference electron density map of I2 (blue mesh) is contoured at 3.5 σ. The $F_{o,I1} - F_{o,I2}$ isomorphous difference electron density map (yellow mesh) is contoured at 5 σ.

In this work we showed a novel strategy to purifiy and crystallize a PC in complex with a noncovalent inhibitor. On the basis of these crystals the structural investigation of many other inhibitor−furin complexes is possible by competitive soaking. This strategy will allow the structure guided development of compounds that are highly promising therapeutics for the treatment of cancer as well as of many viral and bacterial infections.[2−4]

METHODS

The coding sequence of human furin was inserted into the plasmid pHLsec[28] and expressed by transient transfection of human embryonic kidney cells. The protein was purified in a three-step chromatography scheme, employing metal affinity chromatography, inhibitor based affinity chromatography,[17] and size exclusion chromatography. Finally a ∼300-fold enrichment of human furin was observed, corresponding to a specific activity of 57 ± 1 u. One unit corresponds to 1 μmol AMC (h × mg)$^{-1}$ released from the peptide pGlu-Arg-Thr-Lys-Arg-AMC (200 μM) at 37 °C in 100 mM Hepes, pH 7.0, 5 mM $CaCl_2$, 0.5% (v/v) TritonX-100. Details of the expression, preparation, kinetic analyses, and thermal denaturation assays are described in Supporting Information.

For crystallization furin was concentrated to 140−150 μM (∼7.5 mg mL^{-1}), and I1 was added to a final concentration of 290 μM. Crystals were grown at 30 °C in 50 mM Tris, pH 8.5, 2.8 M sodium formate and 0.015 mM Cymal-7. For the structural investigation of the complex of furin with I2, crystals were soaked in crystallization solution supplemented with 3 mM of I2. Diffraction data were collected at 100 K at the BESSY-II beamline 14.1 of the Helmholtz-Zentrum Berlin (HZB)[29] and processed with XDS (v.03/2013[30]). Model building was carried out in COOT (v.0.6.2[31]). CNS (v.1.3[32]) was used for refinement of the structures of furin in complex with I1 and I2 up to 2.3 and 2.7 Å resolution, respectively.

ASSOCIATED CONTENT

Supporting Information

Supplementary figures, supplementary tables, and supplementary methods, containing a detailed description of the expression procedure, crystallographic work, enzymatic tests, and thermal denaturation assays. This material is available free of charge via the Internet at http://pubs.acs.org.

Accession Codes

Structure factors and coordinates for the complex structures of human furin in complex with inhibitor I1 and I2 have been deposited to the protein databank (PDB) with the accession codes 4OMC and 4OMD, respectively.

AUTHOR INFORMATION

Corresponding Author

*E-mail: than@fli-leibniz.de.

Notes

The authors declare no competing financial interest.

ACKNOWLEDGMENTS

We acknowledge the Helmholtz Zentrum Berlin BESSY II for provision of synchrotron radiation at the beamline BL 14.1 and thank the scientific staff for assistance. This work was supported by EMBO (to S.O.D., ASTF 513 - 2011).

REFERENCES

(1) Siezen, R. J., and Leunissen, J. A. (1997) Subtilases: the superfamily of subtilisin-like serine proteases. *Protein Sci. 6*, 501−523.
(2) Thomas, G. (2002) Furin at the cutting edge: from protein traffic to embryogenesis and disease. *Nat. Rev. Mol. Cell. Biol. 3*, 753−766.
(3) Artenstein, A. W., and Opal, S. M. (2011) Proprotein convertases in health and disease. *N. Engl. J. Med. 365*, 2507−2518.
(4) Seidah, N. G., and Prat, A. (2012) The biology and therapeutic targeting of the proprotein convertases. *Nat. Rev. 11*, 367−383.
(5) Couture, F., D'Anjou, F., and Day, R. (2011) On the cutting edge of proprotein convertase pharmacology: from molecular concepts to clinical applications. *Biomol. Concepts 2*, 421−438.
(6) Zhu, J., Declercq, J., Roucourt, B., Ghassabeh, G. H., Meulemans, S., Kinne, J., David, G., Vermorken, A. J., Van de Ven, W. J., Lindberg, I., Muyldermans, S., and Creemers, J. W. (2012) Generation and

characterization of non-competitive furin-inhibiting nanobodies. *Biochem. J. 448*, 73−82.
(7) Lopez de Cicco, R., Bassi, D. E., Zucker, S., Seidah, N. G., and Klein-Szanto, A. J. (2005) Human carcinoma cell growth and invasiveness is impaired by the propeptide of the ubiquitous proprotein convertase furin. *Cancer Res. 65*, 4162−4171.
(8) Coppola, J. M., Bhojani, M. S., Ross, B. D., and Rehemtulla, A. (2008) A small-molecule furin inhibitor inhibits cancer cell motility and invasiveness. *Neoplasia (N. Y., NY, U. S.) 10*, 363−370.
(9) Hallenberger, S., Bosch, V., Angliker, H., Shaw, E., Klenk, H. D., and Garten, W. (1992) Inhibition of furin-mediated cleavage activation of HIV-1 glycoprotein gp160. *Nature 360*, 358−361.
(10) Becker, G. L., Sielaff, F., Than, M. E., Lindberg, I., Routhier, S., Day, R., Lu, Y., Garten, W., and Steinmetzer, T. (2010) Potent inhibitors of furin and furin-like proprotein convertases containing decarboxylated P1 arginine mimetics. *J. Med. Chem. 53*, 1067−1075.
(11) Sarac, M. S., Peinado, J. R., Leppla, S. H., and Lindberg, I. (2004) Protection against anthrax toxemia by hexa-D-arginine in vitro and in vivo. *Infection Immunity 72*, 602−605.
(12) Shiryaev, S. A., Remacle, A. G., Ratnikov, B. I., Nelson, N. A., Savinov, A. Y., Wei, G., Bottini, M., Rega, M. F., Parent, A., Desjardins, R., Fugere, M., Day, R., Sabet, M., Pellecchia, M., Liddington, R. C., Smith, J. W., Mustelin, T., Guiney, D. G., Lebl, M., and Strongin, A. Y. (2007) Targeting host cell furin proprotein convertases as a therapeutic strategy against bacterial toxins and viral pathogens. *J. Biol. Chem. 282*, 20847−20853.
(13) Henrich, S., Cameron, A., Bourenkov, G. P., Kiefersauer, R., Huber, R., Lindberg, I., Bode, W., and Than, M. E. (2003) The crystal structure of the proprotein processing proteinase furin explains its stringent specificity. *Nat. Struct. Biol. 10*, 520−526.
(14) Holyoak, T., Wilson, M. A., Fenn, T. D., Kettner, C. A., Petsko, G. A., Fuller, R. S., and Ringe, D. (2003) 2.4 A resolution crystal structure of the prototypical hormone-processing protease Kex2 in complex with an Ala-Lys-Arg boronic acid inhibitor. *Biochemistry 42*, 6709−6718.
(15) Becker, G. L., Lu, Y., Hardes, K., Strehlow, B., Levesque, C., Lindberg, I., Sandvig, K., Bakowsky, U., Day, R., Garten, W., and Steinmetzer, T. (2012) Highly potent inhibitors of proprotein convertase furin as potential drugs for treatment of infectious diseases. *J. Biol. Chem. 287*, 21992−22003.
(16) Reeves, P. J., Callewaert, N., Contreras, R., and Khorana, H. G. (2002) Structure and function in rhodopsin: high-level expression of rhodopsin with restricted and homogeneous N-glycosylation by a tetracycline-inducible N-acetylglucosaminyltransferase I-negative HEK293S stable mammalian cell line. *Proc. Natl. Acad. Sci. U.S.A. 99*, 13419−13424.
(17) Kuester, M., Becker, G. L., Hardes, K., Lindberg, I., Steinmetzer, T., and Than, M. E. (2011) Purification of the proprotein convertase furin by affinity chromatography based on PC-specific inhibitors. *Biol. Chem. 392*, 973−981.
(18) Krissinel, E., and Henrick, K. (2004) Secondary-structure matching (SSM), a new tool for fast protein structure alignment in three dimensions. *Acta Crystallogr. 60*, 2256−2268.
(19) Henrich, S., Lindberg, I., Bode, W., and Than, M. E. (2005) Proprotein convertase models based on the crystal structures of furin and kexin: explanation of their specificity. *J. Mol. Biol. 345*, 211−227.
(20) Creemers, J. W., Choquet, H., Stijnen, P., Vatin, V., Pigeyre, M., Beckers, S., Meulemans, S., Than, M. E., Yengo, L., Tauber, M., Balkau, B., Elliott, P., Jarvelin, M. R., Van Hul, W., Van Gaal, L., Horber, F., Pattou, F., Froguel, P., and Meyre, D. (2012) Heterozygous mutations causing partial prohormone convertase 1 deficiency contribute to human obesity. *Diabetes 61*, 383−390.
(21) Than, M. E., Henrich, S., Bourenkov, G. P., Bartunik, H. D., Huber, R., and Bode, W. (2005) The endoproteinase furin contains two essential Ca2+ ions stabilizing its N-terminus and the unique S1 specificity pocket. *Acta Crystallogr. 61*, 505−512.
(22) Zheng, H., Chordia, M. D., Cooper, D. R., Chruszcz, M., Muller, P., Sheldrick, G. M., and Minor, W. (2014) Validation of metal-binding sites in macromolecular structures with the CheckMyMetal web server. *Nat. Protoc. 9*, 156−170.
(23) Wheatley, J. L., and Holyoak, T. (2007) Differential P1 arginine and lysine recognition in the prototypical proprotein convertase Kex2. *Proc. Natl. Acad. Sci. U.S.A. 104*, 6626−6631.
(24) Wells, C. M., and Di Cera, E. (1992) Thrombin is a Na(+)-activated enzyme. *Biochemistry 31*, 11721−11730.
(25) Di Cera, E. (2004) Thrombin: a paradigm for enzymes allosterically activated by monovalent cations. *C. R. Biol. 327*, 1065−1076.
(26) Gros, P., Kalk, K. H., and Hol, W. G. (1991) Calcium binding to thermitase. Crystallographic studies of thermitase at 0, 5, and 100 mM calcium. *J. Biol. Chem. 266*, 2953−2961.
(27) Tian, S., Huang, Q., Fang, Y., and Wu, J. (2011) FurinDB: A database of 20-residue furin cleavage site motifs, substrates and their associated drugs. *Int. J. Mol. Sci. 12*, 1060−1065.
(28) Aricescu, A. R., Lu, W., and Jones, E. Y. (2006) A time- and cost-efficient system for high-level protein production in mammalian cells. *Acta Crystallogr. 62*, 1243−1250.
(29) Mueller, U., Darowski, N., Fuchs, M. R., Forster, R., Hellmig, M., Paithankar, K. S., Puhringer, S., Steffien, M., Zocher, G., and Weiss, M. S. (2012) Facilities for macromolecular crystallography at the Helmholtz-Zentrum Berlin. *J. Synchrotron Radiat. 19*, 442−449.
(30) Kabsch, W. (2010) Xds. *Acta Crystallogr. 66*, 125−132.
(31) Emsley, P., Lohkamp, B., Scott, W. G., and Cowtan, K. (2010) Features and development of Coot. *Acta Crystallogr. 66*, 486−501.
(32) Brunger, A. T. (2007) Version 1.2 of the Crystallography and NMR system. *Nat. Protoc. 2*, 2728−2733.